Magnetic Resonance in Medicine 63:1575–1582 (2010)

Estimation of Global Aortic Pulse Wave Velocity by Flow-Sensitive 4D MRI

Michael Markl,[1]* Wolf Wallis,[2] Stefanie Brendecke,[2] Jan Simon,[2] Alex Frydrychowicz,[1] and Andreas Harloff[2]

The aim of this study was to determine the value of flow-sensitive four-dimensional MRI for the assessment of pulse wave velocity as a measure of vessel compliance in the thoracic aorta. Findings in 12 young healthy volunteers were compared with those in 25 stroke patients with aortic atherosclerosis and an age-matched normal control group (n = 9). Results from pulse wave velocity calculations incorporated velocity data from the entire aorta and were compared to those of standard methods based on flow waveforms at only two specific anatomic landmarks. Global aortic pulse wave velocity was higher in patients with atherosclerosis (7.03 ± 0.24 m/sec) compared to age-matched controls (6.40 ± 0.32 m/sec). Both were significantly (P < 0.001) increased compared to younger volunteers (4.39 ± 0.32 m/sec). Global aortic pulse wave velocity in young volunteers was in good agreement with previously reported MRI studies and catheter measurements. Estimation of measurement inaccuracies and error propagation analysis demonstrated only minor uncertainties in measured flow waveforms and moderate relative errors below 16% for aortic compliance in all 46 subjects. These results demonstrate the feasibility of pulse wave velocity calculation based on four-dimensional MRI data by exploiting its full volumetric coverage, which may also be an advantage over standard two-dimensional techniques in the often-distorted route of the aorta in patients with atherosclerosis. Magn Reson Med 63:1575–1582, 2010. © 2010 Wiley-Liss, Inc.

Key words: pulse wave velocity; compliance; phase contrast; atherosclerosis; aorta

Increased pulse wave velocity (PWV) as a measure of aortic stiffness is an important marker for both age-related changes in aortic compliance and the presence of atherosclerosis (1,2) and is an independent predictor of cardiovascular mortality and stroke (3,4). Reliable measurement of PWV is of particular interest for monitoring the progression or regression of vessel compliance during therapy (5,6).

Pressure catheter measurements can be considered the gold standard for the assessment of the development of aortic pressure wave, but their use is limited due to the invasiveness of the procedure (7). To provide a noninvasive estimate of PWV, phase contrast (PC) MRI has been applied in a number of in vivo studies determining blood flow based on flow waveform measurements in single two-dimensional (2D) planes transecting the aorta (8–10). For PWV estimation, typically transit-time methods are employed estimating temporal differences of specific features of blood flow waveforms, e.g., time from foot to foot or peak to peak, between two locations of the vessel with known distance (11–24). However, the precision of this method highly depends on the exact calculation of flow difference and distance between only two measuring points (16,25,26).

Methodological improvements include a more continuous evaluation along a vessel center line and cross-correlation (XCor) analysis for the estimation of waveform delays, which improved the accuracy of PWV estimation but relied on 2D PC acquisitions in sagittal oblique slices exactly transecting the thoracic aorta (27,28). Recently, more comprehensive three-dimensional (3D) CINE techniques in combination with three-directionally encoded velocities (flow-sensitive four-dimensional [4D] MRI) have been reported that provide information on multidirectional in vivo blood flow with full volumetric coverage of the vessel of interest (29–34). It was the purpose of this study to investigate if PWV can be reliably estimated from 3D CINE PC data despite its lower temporal resolution by exploiting its full volumetric coverage. In addition, flow-sensitive 4D MRI may be advantageous in patients with complex aortic shapes that cannot be covered by a single 2D analysis plane.

Our method was based on multiple pulsatile flow waveforms, retrospectively extracted from flow-sensitive 4D MR data, and distributed homogenously with 10 mm gaps along the entire course of the thoracic aorta. PWV was determined by transit-time methods and the linear fit from data of the entire aorta.

Global and regional changes of PWV were analyzed in a study of 12 healthy volunteers, 25 stroke patients with aortic atherosclerosis, and nine age-matched subjects without atherosclerotic disease. Flow profiles were used to compare different PWV estimation methods and to evaluate the sensitivity to detect changes in aortic compliance related to age and the presence of atherosclerosis.

MATERIALS AND METHODS

Human Subjects

After ethical approval and written informed consent, 12 healthy volunteers (24.5 ± 3.2 years) and 25 patients (66.1 ± 7.8 years), were included in the study. In all

[1]Department of Radiology, Medical Physics, University Hospital, Albert-Ludwigs-Universität Freiburg, Freiburg, Germany.

[2]Department of Neurology, University Hospital, Albert-Ludwigs-Universität Freiburg, Freiburg, Germany.

*Correspondence to: Michael Markl, Ph.D., University Hospital Freiburg, Department of Radiology, Medical Physics, Hugstetter Strasse 55, 79106 Freiburg, Germany. E-mail: michael.markl@uniklinik-freiburg.de

Received 9 February 2009; revised 18 November 2009; accepted 14 December 2009.

DOI 10.1002/mrm.22353

Published online in Wiley InterScience (www.interscience.wiley.com).

Table 1
Baseline Characteristics of the Study Participants*

Characteristic		Young volunteers	Age-matched volunteers	Patients
Number	*n*	12	9	25
Age (years)	Mean ± SD	24.5 ± 3.2	64.2 ± 7.8	66.1 ± 7.8
	Range	20–33	54–74	44–74
Female sex	*n* (%)	3 (25)	3 (33)	12 (48)
Maximum AWT in transesophageal echocardiography (mm)	Mean ± SD	N/A	2.5 ± 0.3	4.1 ± 0.8
	Range		1.9–2.9	3.0–5.8
Mean aortic diameter (mm)	Mean ± SD	25.5 ± 1.8,	27.6 ± 2.1	28.3 ± 2.8,
	Range	22.7–28.3	24.0–30.0	22.3–34.0
Number of analysis planes in thoracic aorta (*n*)	Mean ± SD	31.9 ± 2.9	30.4 ± 3.1	32.1 ± 5.3
	Range	27–37	23–35	25–41

*AWT: aortic wall thickness; TTE: transesophageal echocardiography.

patients, transesophageal echocardiography was used to confirm the presence of aortic plaques ≥3 mm. In addition, nine age-matched controls (64.2 ± 7.8 years) without cardiovascular disease and nonatherosclerosis (aortic plaques <3 mm in transesophageal echocardiography) were included. Patients and volunteer demographics are summarized in Table 1.

MRI Measurements

All measurements were performed on a 3-T MR system (TRIO; Siemens, Erlangen, Germany) using a standard 12-channnel body coil. ECG-synchronized (prospective gating) and respiration-controlled (navigator gating) flow-sensitive MRI was performed using a sagittal oblique 3D volume covering the entire thoracic aorta, as described previously (32,34). The pulse sequence consisted of a rf-spoiled gradient echo sequence with three-directional velocity encoding (venc = 150 cm/sec along all directions). Scan parameters were as follows: echo time/repetition time = 2.6–3.5 ms/5.1–6.1 ms, flip angle = 7–15°, temporal resolution = 40.8 ms, spatial resolution = 1.7 × 2.0 × 2.2 mm^3. Total acquisition time for flow-sensitive MRI depends on heart rate, and navigator gating efficiency and was of the order of 15 to 20 min.

Data Analysis

All acquired 46 flow-sensitive 4D MR data sets were corrected for velocity aliasing and eddy currents and Maxwell terms. The 4D data were used to calculate a time-averaged 3D PC MR angiography, as described before (34), and to position a series of virtual 2D emitter planes along the entire thoracic aorta. To guarantee comparability of the results between different subjects, an initial plane #0 was positioned directly distal to the outlet of the left subclavian artery. Subsequently, all other 2D analysis planes were manually positioned and carefully angulated upstream and downstream in 10 mm intervals. For the positioning of each new analysis plane, the plane location was automatically shifted by a distance of 10 mm normal to the previous analysis plane and then angulated normal to the aortic lumen at the new location (for details see also Fig. 1). 3D blood flow visualization (time-resolved 3D vector graphs; EnSight v. 8.2, CEI, Apex, NC, USA) was used to provide a visual impression of the propagation of the pulsatile flow waveforms along the aorta during the cardiac cycle (Figs. 1 and 7).

For each analysis plane, the boundaries of the 3D PC-MRA were used to define the aortic lumen contour, as shown in Fig. 1 (right column). The temporal evolution of blood flow for each analysis plane was calculated by multiplying the lumen area with the mean absolute velocity inside the lumen for each time frame in the cardiac cycle.

PWV was derived from the data by automatically identifying the time to peak (TTP) and time to foot (TTF) of the flow waveform, as illustrated in Fig. 2a. TTF was extracted from the flow waveforms by fitting a line to the upslope portion of the waveform (between 20% and 80% of the peak flow) and was defined as the intersection of the fitted line with the zero line. PWV was then determined by plotting the resulting TTP or TTF of all evaluated analysis planes as a function of location along the aortic lumen (Fig. 2b). In addition, XCor as recently proposed by Fielden et al. (28) was used to estimate the temporal differences between the velocity-time curves in different analysis planes. Briefly, the waveform at each location was compared to the waveform of the first analysis plane in the ascending aorta (plane #12 in Fig. 1). A cross-correlation function was used to apply a time shift to the more distal waveforms until the highest correlation value between the two waveforms was obtained, returning a time shift for each analysis plane relative to the first location.

For all three analysis methods (TTF, TTP, and XCor), the global PWV of the entire thoracic aorta was calculated as the inverse of the slope of a linear fit to the data. For volunteers, results were compared to standard methods by estimating PWV based on TTP, TTF, and XCor in two analysis planes in the ascending and descending aorta, separated by a distance of 200 mm.

Statistical Analysis

All continuous values regarding the comparison of the different analysis methods are reported as mean ± 1 standard deviation (SD). To account for the different numbers of subjects in three analyzed populations (young controls, age-matched controls, and patients), the mean ± standard error was used for comparing results between groups. To detect statistically significant differences between the PWV distributions between two populations, the Mann-Whitney *U* test was employed. All tests used a significance level of 5%.

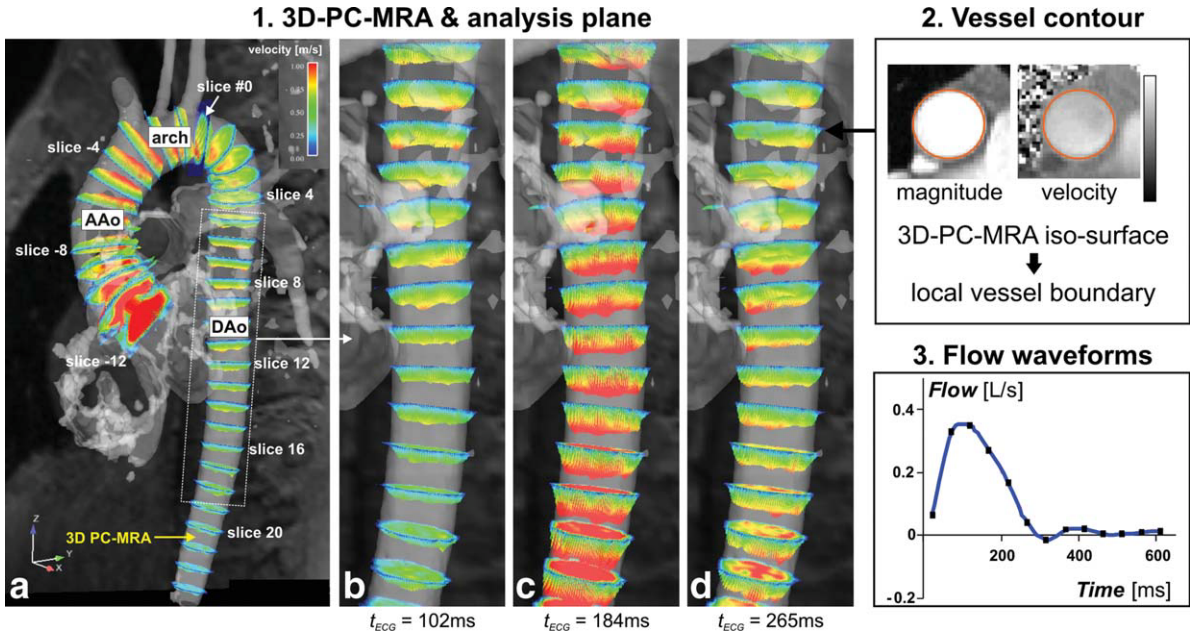

FIG. 1. **a:** Visualization of pulse wave propagation within the thoracic aorta, based on flow-sensitive 4D MRI data. Equidistant analysis planes with an interanalysis plane gap of 10 mm were positioned upstream (negative analysis plane numbers) and downstream (positive analysis plane numbers) along the thoracic aorta, starting with analysis plane #0 (outlet of the left subclavian artery). **b–d:** Spatially varying flow profiles from the proximal to the distal DAo in analysis planes can be appreciated in successive systolic time frames: during early systole (**b**), profiles in the proximal DAo are already fully developed, while velocities are continuously lower further downstream. During peak systole (**c**), flow profiles reach their maxima in the entire DAo, while during late systole (**d**), flow profiles in the proximal DAo are already reduced compared to flow further downstream. 2. The boundaries of the derived 3D PC MR-angiography (PC-MRA) were used to automatically define the local vessel boundaries and lumen area. 3. Resulting flow waveform. AAo: ascending aorta, DAo: descending aorta.

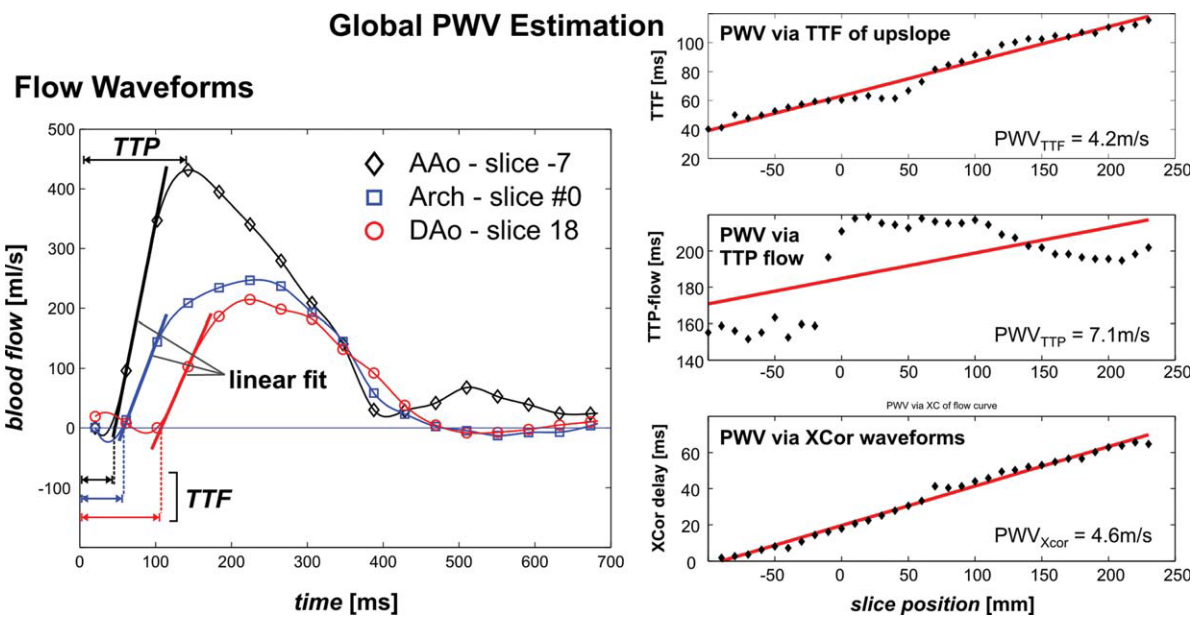

FIG. 2. **a:** Sample flow waveforms in analysis planes in the ascending aorta (AAo), arch, and descending aorta (DAo). **b:** TTP and TTF were automatically extracted from the measured flow waveforms. XCor analysis provided time delays between the flow waveforms of the most proximal and all other analysis planes. Each method was used for the estimation of global PWV by linearly fitting data from all evaluated analysis planes in the thoracic aorta.

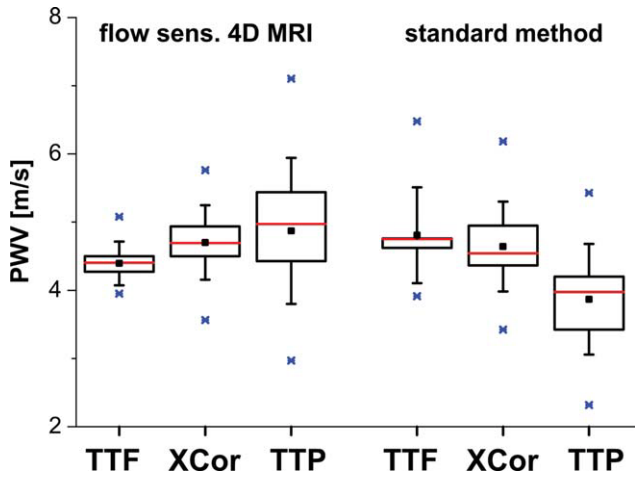

FIG. 3. Box plot of the PWV of normal volunteers calculated with different methods (TTP, TTF, XCor). The statistics are based on values for 12 volunteers. Small filled box = mean, red line = median; large box = [25,75]% of the data; error bars = SD, blue x = min and max values within [1,99]% of the data.

RESULTS

MRI Measurements

Depending on geometry and size of the aorta, up to 41 analysis planes (see also Table 1) were positioned in the thoracic aorta (Fig. 1). 3D visualization using vector graphs for each analysis plane was applied to visually identify spatial and temporal propagation of flow profiles. Such changes reflecting the traveling pulse wave during systole can be appreciated by comparing velocity profiles at different temporal and spatial levels within the aorta, as shown in the magnified descending aorta in Fig. 1b–d.

PWV Analysis Methods

In accordance with previously published work (7,28) and as shown in Fig. 2b, PWV analysis based on TTF and XCor provided more stable estimations of waveform changes along the path of the aorta (i.e., less scattered data) if compared to TTP. These findings are also reflected in the cumulative results of all 12 volunteers, as shown in Fig. 3. If the results from the different PWV calculation methods are directly compared, it is obvious that PWV estimation based on TTF and 4D data demonstrated lowest data variability, mirrored by smaller standard and overall data range. In contrast, PWV estimation based on TTP using 4D data or the standard technique with two analysis planes in the ascending and descending aorta showed substantially greater data variability for the same group of volunteers. Analysis based on TTF was also mildly superior to calculations based on the XCor technique. Values for normal global PWV based on TTF and 4D data (mean = 4.39 ± 0.32 m/sec) were in close agreement with results from previous studies listed in Table 2 (3–5). Therefore, all further analysis of global and regional PWV was based on the TTF method.

PWV in Patients With Atherosclerosis, Age-Matched Controls, and Healthy Volunteers

As shown in Fig. 4a, global PWV in patients with atherosclerosis was increased (7.03 ± 0.24 m/sec; range, 4.35 to 9.21 m/sec) compared to an age-matched control group (6.40 ± 0.32 m/sec; range, 4.94 to 8.20 m/sec) beyond the standard error. However, the statistical comparison of the two populations did not demonstrate a significant difference ($P = 0.13$). For both patients and age-matched controls, PWV was significantly ($P < 0.001$) higher and varied more widely compared to global PWV in the younger group of 12 volunteers (4.39 ± 0.09 m/sec; range, 3.95 to 5.08 m/sec). In addition, a high correlation of increasing global PWV with increasing age could be demonstrated (Fig. 4b).

Error Propagation Analysis

Results from a previous study of the aorta in 20 normal volunteers (35) showed that the noise level of the velocities obtained from flow-sensitive 4D MRI with a velocity sensitivity of 150 cm/sec was $\sigma_V = 1.22$ cm/sec. Based on the spatial resolution of the measured data (~2 mm^2) a systematic error of $\Delta d = \pm 2$ mm regarding the aortic lumen diameter d was assumed.

Error propagation results in an uncertainty of $\Delta A = \pi/2\, d\, \Delta d$ for the lumen area and thus final uncertainty of the flow rate of $\Delta F = \mathrm{sqrt}(\Delta A^2 + \sigma_V^2)$. The aortic lumen diameters in our study, ranging from 22.3 to 34.0 mm (see Table 1), resulted in only minimal flow measurement uncertainties within 1.4 mL/sec < ΔF < 1.62 mL/sec.

Due to the small uncertainty ΔF of the flow waveforms, we assumed that the potential timing error ΔTTF in detecting the foot of the flow waveform was relatively

Table 2
Normal Global Pulse Wave Velocities Found in Our Study Compared to Previously Published Results*

Study	Method	Normal subjects	Age (years)	Global PWV (m/sec)
Present study	Flow-sensitive 4D MRI multiple analysis planes	$n = 12$	25 ± 3	4.4 ± 0.3
Fielden et al., 2008 (28)	2D PC-MRI sagittal slice and centerline	$n = 13$	29 ± 7	4.5 ± 0.5
Yu et al., 2006 (27)	2D PC-MRI sagittal slice and centerline	$n = 17$	34 ± 11	5.4 ± 0.9 (distal DAo)
Vulliemoz et al., 2002 (18)	2D PC-MRI, two slices in AAo and DAo	$n = 10$	34	4.4 ± 0.9
Latham et al., 1985 (7)	Catheter invasive pressure measurement	$n = 9$	42 ± 5	5.0 ± 0.5

*PWV from catheter measurements (Latham et al. (7), last row) were determined as the TTF differences of aortic pressure waveforms taken at different location in the thoracic aorta. AAo: ascending aorta; DAo: descending aorta.

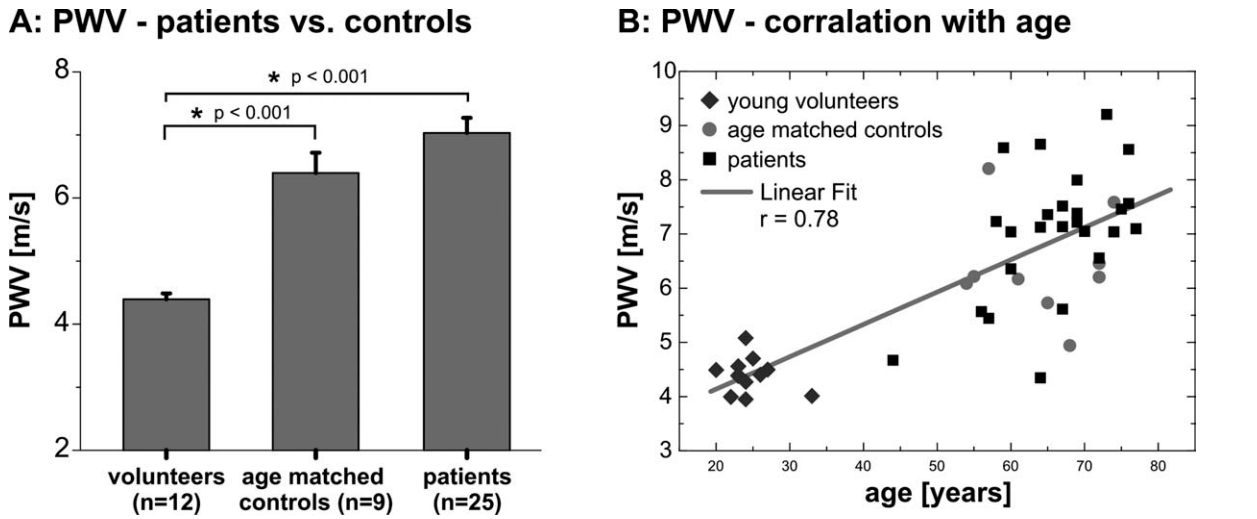

FIG. 4. **a:** Average PWV of normal volunteers compared to patients and age-matched controls demonstrating an increase of PWV in presence of atherosclerosis (error bars = standard errors). **b:** PWV for all subjects included in the study ($n = 46$) as a function of age. In addition to a clear increase in PWV for patients compared to volunteers, a systematic increase of PWV with increasing age can be observed.

small and on the order of $\Delta TTF = \pm 5$ ms. The linear fit (see Fig. 2) would thus result in different inaccuracies of the slope of the TTF data, depending on the number of $N_A = 23$–41 analysis planes used for the individual subject (see also Table 1). Improved performance is achieved for larger numbers of analysis planes.

The resulting error ΔPWV_{TTF} for the TTF method was calculated for each subject based on the individual number of analysis planes and $\Delta TTF = \pm 5$ ms, assuming an error of the fitted line slope of $\Delta slope = \Delta TTF/(N_A 10$ mm). Error propagation resulted in 0.24 m/sec $< \Delta PWV_{TTF} <$ 1.37m/sec for the PWV_{TTF} in the range of 3.91 m/sec to 9.21 m/sec in this study. A more detailed illustration of the distribution of the PWV_{TTF} uncertainties (relative errors = $\Delta PWV_{TTF}/PWV_{TTF}$), which were below 16% for all 46 subjects, is provided in Fig. 5.

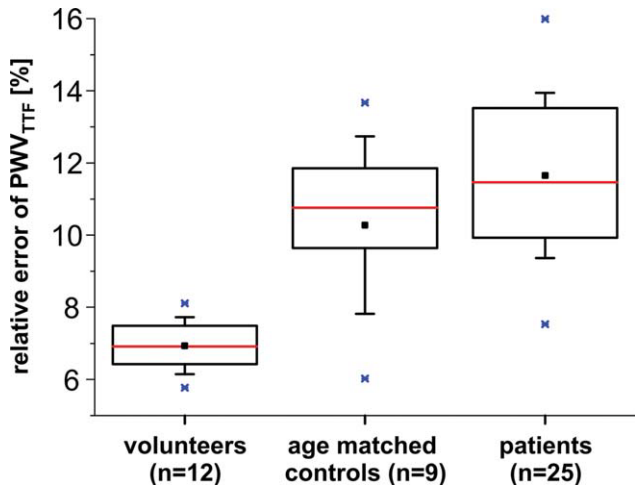

FIG. 5. Relative errors of PWV estimation based on the TTF method for all young volunteers, age-matched controls, and patients. Small filled box = mean, red line = median; large box = [25,75]% of the data; error bars = SD, blue x = min and max values within [1,99]% of the data. [Color figure can be viewed in the online issue, which is available at www.interscience.wiley.com.]

DISCUSSION

The results of the present study demonstrate the feasibility of flow-sensitive 4D MRI for the estimation of normal and pathologic PWV. It should be noted that the presented method requires quite long scan times, which may be considerably longer compared to 2D CINE PC techniques. The reliability of 2D CINE PC for the assessment of PWV has been shown in a number of studies and it constitutes a valid method for the estimation of aortic elasticity. It was not the purpose of our study to demonstrate the superiority of flow-sensitive 4D MRI compared to 2D CINE PC but to show that PWV can also be reliably estimated from flow-sensitive 4D MRI data despite its lower temporal resolution by exploiting its full volumetric coverage. To compensate for resulting uncertainties, time of travel between two neighboring planes PWV was not calculated from pairs of planes but rather by including all analysis planes and line fitting in the final PWV estimation.

To define a consistent measure of PWV, analysis was based on a series of emitter planes. Since moderate angulations in the ascending aorta and arch and only minimal angulations in the descending were necessary for positioning of successive analysis planes, potential inaccuracies of interanalysis plane distances were assumed to be negligible. In addition, such errors are expected to be less severe if PWV is estimated by fitting data points from a large number of analysis planes.

Despite similar mean values for all volunteers, the increased data range using TTP indicates inconsistent and less reliable assessment of temporal differences in flow waveforms, most likely due to reflected pressure waves, which can influence the timing of peak velocities, particularly in the descending aorta, as reported previously (3). In contrast, TTF represents flow

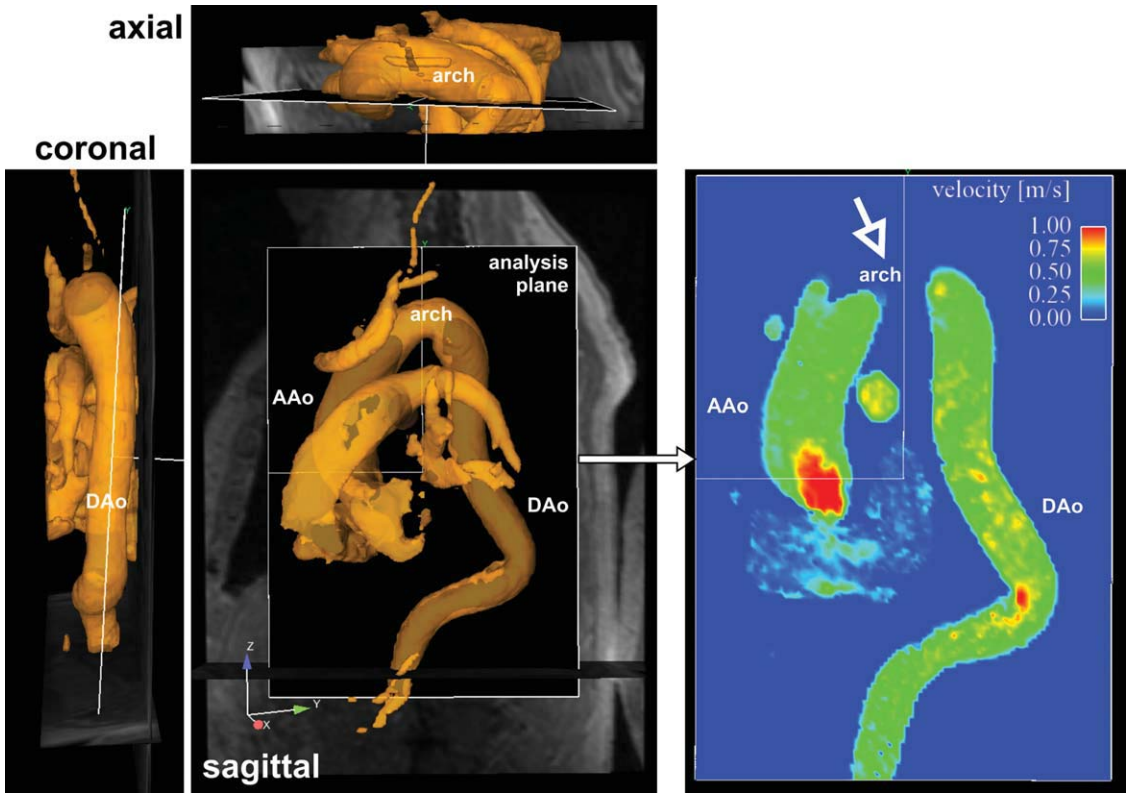

FIG. 6. Aortic geometry shown as 3D PC-MRA isosurface in sagittal, coronal, and axial orientation of a patient with complex shape of the thoracic aorta. In this case, an oblique sagittal slice cannot be angulated in such a way that the full thoracic aortic lumen can be included into a single analysis plane. Despite full coverage of the ascending (AAo) and descending aorta (DAo), velocities cannot be assessed in the aortic arch (open white arrow).

waveform changes during early systole and is less likely affected by such drawbacks since reflection waves need a finite time to reach the aorta from the periphery. Analysis based on XCor provided similar results but was slightly less stable compared to the TTF methods, contrary to findings in a previous study (28). However, the results of both studies cannot be directly compared since different data acquisition strategies (2D and vessel centerline versus 4D coverage and multiple analysis planes) and imaging parameters (temporal resolution) were used.

Based on our cohort of young volunteers, patients with proven atherosclerosis of the aorta, and age-matched controls, the effects of age on changes in PWV could be evaluated. In patients with aortic atherosclerosis as

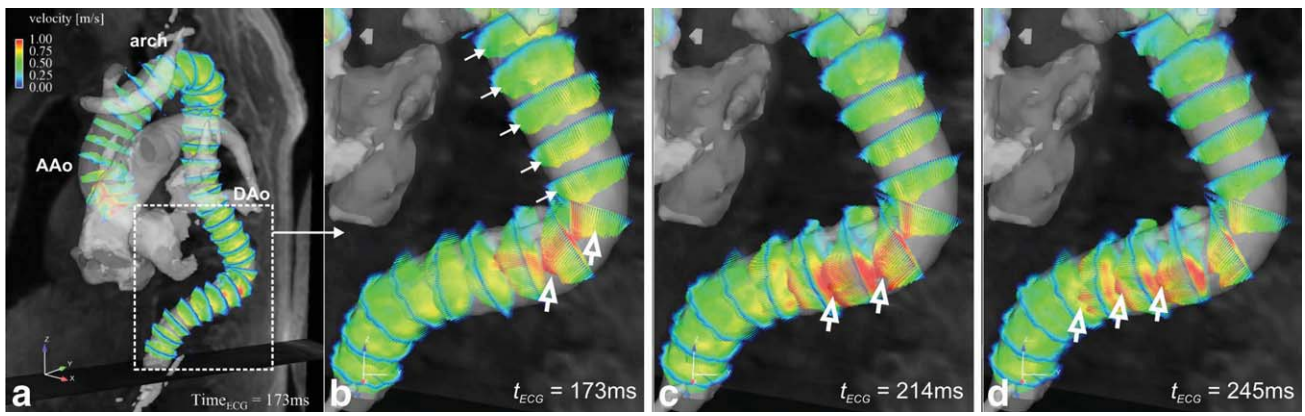

FIG. 7. Pulse wave velocity estimation in a patient with substantial elongation and rotation of the descending aorta (A). The strong bending of the DAo leads to local flow acceleration (red colored vectors) and delayed passage of blood through the bend. While flow profiles proximal to the bend already reach their maximum during early systole (B, solid white arrows), peak flow in and distal to the bend develop more gradually over a longer period of time as illustrated by the open arrows in BD.

confirmed by transesophageal echocardiography, the expected increase of global PWV and age-related reduction of aortic compliance could be clearly confirmed with our technique.

The direct comparisons of patients with atherosclerosis and the age-matched control populations did not result in a significant difference ($P = 0.13$). The analysis presented in this study could therefore not prove a significant acceleration of PWV in atherosclerosis. We speculate that the small size of the age-matched control group may have led to this result and larger populations may be needed to identify significant changes in PWV.

A limitation of this study is related to potential inaccuracies related to velocity noise and lumen segmentation errors. In addition, the temporal resolution of 40 ms was lower than in previous studies (18,27,28) and may not be sufficient to reliably detect the rapid waveform changes associated with typical pulse wave velocities of the order of 5-10 m/sec and results in uncertainties in the estimation of the foot of the waveform delays. To compensate for the low temporal resolution, PWV was determined by a fit to all calculated timing delays in a large number of analysis planes. Error propagation analysis revealed only minor effects on calculated flow values and relatively moderate uncertainties in the calculated PWV data <16% for all 46 subjects included in this study. Nevertheless, an increase of temporal resolution in future studies using flow-sensitive 4D MRA might improve PWV accuracy.

Although lumen changes during the cardiac cycle will affect the magnitude of the derived flow values, it is expected that the time differences in adjacent pulsatile flow waveforms used from PWV estimation can be assessed with reliable accuracy.

We were currently not able to compare our PWV data obtained from MRI with a reference standard. The only gold standard for PWV measurements would be invasive catheter measurements, which were not performed in our study. However, our data are in excellent agreement with previously published data from MRI studies and, more important, with an earlier study by Latham et al. (7) analyzing regional PWV in normal volunteers based on pressure catheter measurements. In addition, the intrastudy comparisons of results for patients with proven atherosclerosis with findings from age-matched and young volunteers indicate the potential of the method to detect physiologic evolution of PWV with age.

Taking into account the individual anatomy of the thoracic aorta in patients with atherosclerosis is a clear advantage of the presented 3D MRI technique. As an example of the benefit for the full spatial coverage offered by flow sensitive 4D MRI, Figs. 6 and 7 illustrate PWV propagation in a patient with an elongation of the descending aorta. Due to the generally complex shape and distorted route of the vascular lumen, it was not possible to define a single sagittal oblique analysis plane incorporating the entire thoracic aortic lumen, as illustrated in Fig. 6a. In this case, previously reported methods relying on in-plane velocity measurements and evaluation of PWV along a vessel centerline (29–34) are no longer applicable. Note also that the complex aortic shape and in particular the sharp bending of the distal descending aorta in this patient (see Fig. 7) resulted in reduced transit times of the flow waveforms while global PWV was still high (7 m/sec). Based on these observations, a more detailed correlation to aortic shape, aortic diameter, and resulting PWV may be needed in future studies.

In summary, flow-sensitive 4D MRI in conjunction with multiplanar analysis of pulsatile flow waveforms permits an estimation of global aortic PWV in volunteers and patients with advanced aortic disease. A significant correlation of aortic elasticity with age and thus higher vessel stiffness and good agreement with the existing literature were demonstrated.

ACKNOWLEDGMENTS

Michael Markl and Andreas Harloff are supported by the Deutsche Forschungsgemeinschaft (DFG), Grant MA 2383/4-1. Michael Markl is supported by the Bundesministerium für Bildung und Forschung (BMBF), Grant 01EV0706.

REFERENCES

1. Farrar DJ, Bond MG, Riley WA, Sawyer JK. Anatomic correlates of aortic pulse wave velocity and carotid artery elasticity during atherosclerosis progression and regression in monkeys. Circulation 1991; 83:1754–1763.
2. Mohiaddin RH, Longmore DB. MRI studies of atherosclerotic vascular disease: structural evaluation and physiological measurements. Br Med Bull 1989;45:968–990.
3. Laurent S, Katsahian S, Fassot C, Tropeano AI, Gautier I, Laloux B, Boutouyrie P. Aortic stiffness is an independent predictor of fatal stroke in essential hypertension. Stroke 2003;34:1203–1206.
4. Nurnberger J, Kribben A, Philipp T, Erbel R. [Arterial compliance (stiffness) as a marker of subclinical atherosclerosis]. Herz 2007;32: 379–386.
5. Kronzon I, Tunick PA. Aortic atherosclerotic disease and stroke. Circulation 2006;114:63–75.
6. Laurent S, Cockcroft J, Van Bortel L, Boutouyrie P, Giannattasio C, Hayoz D, Pannier B, Vlachopoulos C, Wilkinson I, Struijker-Boudier H. Expert consensus document on arterial stiffness: methodological issues and clinical applications. Eur Heart J 2006;27: 2588–2605.
7. Latham RD, Westerhof N, Sipkema P, Rubal BJ, Reuderink P, Murgo JP. Regional wave travel and reflections along the human aorta: a study with six simultaneous micromanometric pressures. Circulation 1985;72:1257–1269.
8. Moran PR. A flow velocity zeugmatographic interlace for NMR imaging in humans. Magn Reson Imaging 1982;1:197–203.
9. Underwood SR, Firmin DN, Klipstein RH, Rees RS, Longmore DB. Magnetic resonance velocity mapping: clinical application of a new technique. Br Heart J 1987;57:404–412.
10. Pelc NJ, Herfkens RJ, Shimakawa A, Enzmann DR. Phase contrast cine magnetic resonance imaging. Magn Reson Q 1991;7: 229–254.
11. Dumoulin CL, Doorly DJ, Caro CG. Quantitative measurement of velocity at multiple positions using comb excitation and Fourier velocity encoding. Magn Reson Med 1993;29:44–52.
12. Groenink M, de Roos A, Mulder BJ, Spaan JA, van der Wall EE. Changes in aortic distensibility and pulse wave velocity assessed with magnetic resonance imaging following beta-blocker therapy in the Marfan syndrome. Am J Cardiol 1998;82:203–208.
13. Lehmann ED. Noninvasive measurements of aortic stiffness: methodological considerations. Pathol Biol (Paris) 1999;47:716–730.
14. Boese JM, Bock M, Schoenberg SO, Schad LR. Estimation of aortic compliance using magnetic resonance pulse wave velocity measurement. Phys Med Biol 2000;45:1703–1713.
15. Rogers WJ, Hu YL, Coast D, Vido DA, Kramer CM, Pyeritz RE, Reichek N. Age-associated changes in regional aortic pulse wave velocity. J Am Coll Cardiol 2001;38:1123–1129.

16. Stevanov M, Baruthio J, Gounot D, Grucker D. In vitro validation of MR measurements of arterial pulse-wave velocity in the presence of reflected waves. J Magn Reson Imaging 2001;14:120–127.
17. Metafratzi ZM, Efremidis SC, Skopelitou AS, De Roos A. The clinical significance of aortic compliance and its assessment with magnetic resonance imaging. J Cardiovasc Magn Reson 2002;4:481–491.
18. Vulliemoz S, Stergiopulos N, Meuli R. Estimation of local aortic elastic properties with MRI. Magn Reson Med 2002;47:649–654.
19. Oliver JJ, Webb DJ. Noninvasive assessment of arterial stiffness and risk of atherosclerotic events. Arterioscler Thromb Vasc Biol 2003;23: 554–566.
20. Gang G, Mark P, Cockshott P, Foster J, Martin T, Blyth K, Steedman T, Elliott A, Dargie H, Groenning B. Measurement of pulse wave velocity using magnetic resonance imaging. Conf Proc IEEE Eng Med Biol Soc 2004;5:3684–3687.
21. Shao X, Fei DY, Kraft KA. Rapid measurement of pulse wave velocity via multisite flow displacement. Magn Reson Med 2004;52: 1351–1357.
22. Gatehouse PD, Keegan J, Crowe LA, Masood S, Mohiaddin RH, Kreitner KF, Firmin DN. Applications of phase-contrast flow and velocity imaging in cardiovascular MRI. Eur Radiol 2005;15:2172–2184.
23. Laffon E, Marthan R, Montaudon M, Latrabe V, Laurent F, Ducassou D. Feasibility of aortic pulse pressure and pressure wave velocity MRI measurement in young adults. J Magn Reson Imaging 2005;21: 53–58.
24. Peng HH, Chung HW, Yu HY, Tseng WY. Estimation of pulse wave velocity in main pulmonary artery with phase contrast MRI: preliminary investigation. J Magn Reson Imaging 2006;24:1303–1310.
25. Bolster BD Jr, Atalar E, Hardy CJ, McVeigh ER. Accuracy of arterial pulse-wave velocity measurement using MR. J Magn Reson Imaging 1998;8:878–888.
26. Bradlow WM, Gatehouse PD, Hughes RL, O'Brien AB, Gibbs JS, Firmin DN, Mohiaddin RH. Assessing normal pulse wave velocity in the proximal pulmonary arteries using transit time: a feasibility, repeatability, and observer reproducibility study by cardiovascular magnetic resonance. J Magn Reson Imaging 2007;25:974–981.
27. Yu HY, Peng HH, Wang JL, Wen CY, Tseng WY. Quantification of the pulse wave velocity of the descending aorta using axial velocity profiles from phase-contrast magnetic resonance imaging. Magn Reson Med 2006;56:876–883.
28. Fielden SW, Fornwalt BK, Jerosch-Herold M, Eisner RL, Stillman AE, Oshinski JN. A new method for the determination of aortic pulse wave velocity using cross-correlation on 2D PCMR velocity data. J Magn Reson Imaging 2008;27:1382–1387.
29. Wigstrom L, Sjoqvist L, Wranne B. Temporally resolved 3D phase-contrast imaging. Magn Reson Med 1996;36:800–803.
30. Buonocore MH. Visualizing blood flow patterns using streamlines, arrows, and particle paths. Magn Reson Med 1998;40:210–226.
31. Bogren HG, Buonocore MH. 4D magnetic resonance velocity mapping of blood flow patterns in the aorta in young vs. elderly normal subjects. J Magn Reson Imaging 1999;10:861–869.
32. Frydrychowicz A, Harloff A, Jung B, Zaitsev M, Weigang E, Bley TA, Langer M, Hennig J, Markl M. Time-resolved, 3-dimensional magnetic resonance flow analysis at 3 T: visualization of normal and pathological aortic vascular hemodynamics. J Comput Assist Tomogr 2007;31:9–15.
33. Hope TA, Markl M, Wigstrom L, Alley MT, Miller DC, Herfkens RJ. Comparison of flow patterns in ascending aortic aneurysms and volunteers using four-dimensional magnetic resonance velocity mapping. J Magn Reson Imaging 2007;26:1471–1479.
34. Markl M, Harloff A, Bley TA, Zaitsev M, Jung B, Weigang E, Langer M, Hennig J, Frydrychowicz A. Time-resolved 3D MR velocity mapping at 3T: improved navigator-gated assessment of vascular anatomy and blood flow. J Magn Reson Imaging 2007; 25:824–831.
35. Stalder AF, Russe MF, Frydrychowicz A, Bock J, Hennig J, Markl M. Quantitative 2D and 3D phase contrast MRI: optimized analysis of blood flow and vessel wall parameters. Magn Reson Med 2008;60: 1218–1231.